Molecular Emission Line Formation in Prestellar Cores

Ya. Pavlyuchenkov[1,2], D. Wiebe[2], B. Shustov[2],

Th. Henning[1], R. Launhardt[1], D. Semenov[1]

ABSTRACT

We investigate general aspects of molecular line formation under conditions which are typical of prestellar cores. Focusing on simple linear molecules, we study formation of their rotational lines by radiative transfer simulations. We present a thermalization diagram to show the effects of collisions and radiation on the level excitation. We construct a detailed scheme (contribution chart) to illustrate the formation of emission line profiles. This chart can be used as an efficient tool to identify which parts of the cloud contribute to a specific line profile. We show how molecular line characteristics for uniform model clouds depend on hydrogen density, molecular column density, and kinetic temperature. The results are presented in a 2D plane to illustrate cooperative effects of the physical factors. We also use a core model with a non-uniform density distribution and chemical stratification to study the effects of cloud contraction and rotation on spectral line maps. We discuss the main issues that should be taken into account when dealing with interpretation and simulation of observed molecular lines.

Subject headings: line: formation — line: profiles — radiative transfer — stars: formation — ISM: clouds

1. Introduction

Star formation is a fundamental process in the universe. Dense, gravitationally bound, and genuinely starless cores, which we call here “prestellar cores”, are the earliest visible precursors of forming stars. The interplay between gravitation and thermal/magnetic pressure as well as the conservation of angular momentum are all driving forces behind prestellar

---

[1]Max Planck Institut für Astronomie, Königstuhl 17, D69117 Heidelberg, Germany;

[2]Institute of Astronomy, Russian Academy of Sciences, Pyatnitskaya 48, Moscow, 109117, Russia

core evolution. While the thermal structure is determined by dust properties and molecular composition, magnetic support is sensitive to the ionization degree. The interaction and relative importance of these processes as well as the role of external forces are still not well understood (see, e.g. reviews by Mac Low & Klessen 2004; Bergin & Tafalla 2007). Thus, it is important to study the physical and chemical evolution of these cores in detail to reveal the underlying physics.

The interiors of such prestellar cores are well-shielded from interstellar or stellar radiation, leading to low internal temperatures. Under such conditions, the main component of these cores, H_2, is not easily observable. Therefore, we have to rely on indirect methods to determine the physical structure of prestellar cores, e.g., on observations of thermal dust emission or emission lines from other molecules, like CO, CS and N_2H^+. Observations of spectral lines have an important advantage over continuum observations since they also carry information about kinematics of the gas. A disadvantage of molecular tracers can be that they are only present under certain conditions and can be frozen-out on dust surfaces. Numerous studies, including single-dish and interferometric observations along with their theoretical analysis, have been performed over the past years, significantly deepening our understanding of the physical and chemical processes in star-forming regions (see, e.g. reviews of Myers 1999; Evans 1999; di Francesco et al. 2007; Bergin & Tafalla 2007). However, deriving physical properties from molecular lines is a difficult (inverse) problem because of the many factors which can affect the line formation.

Even if we assume that the studied object is spherically symmetric and uniform, we have to specify at least 5 independent parameters describing the formation of molecular lines. These are density $n(\mathrm{H_2})$, kinetic temperature $T_{\rm kin}$, molecular column density $N(\mathrm{mol})$, radial velocity V_r, and micro-turbulent velocity $V_{\rm turb}$. In more realistic models, additional parameters should also be considered, e.g., electron concentration and external radiation field, with spatial distributions of all the above parameters.

An exact analytical treatment of this multi-parameter system is, in most cases, impossible. Optically thin line formation can be described analytically to some extent (see, e.g., Rohlfs & Wilson 2000), but it is very difficult to do the same for optically thick lines. Also, it is difficult to use analytic methods to solve the inverse problem, i.e., to restore physical distributions of relevant parameters from observed spectra because of the non-local and non-linear nature of the radiative transfer problem. This is why numerical line radiative transfer (LRT) models are commonly used as an exploratory tool. Several reliable numerical methods and numerical codes have been developed by various groups for this purpose (see reviews by Peraiah 2001; van Zadelhoff et al. 2002). There are also fast approximate numerical tools available for the molecular line radiative transfer analysis[1] (van der Tak et al. 2007). However, input data for line modeling include not only physical conditions but also distributions of molecular abundances. All these data can be represented with some analytical prescription or extracted from chemical and dynamical models.

As recently outlined by Tsamis et al. (2008), there are two alternative approaches to the diagnostics of protostellar objects. The first approach is a systematic study of the influence of various factors on emergent spectra in order to facilitate the analysis of forthcoming observations. Such studies (based mainly on approximate LRT methods) have already started more than 30 years ago with the analysis of the excitation conditions for various molecules and effects of the density, temperature and velocity gradients on the emission line profiles (e.g., Lucas 1974; Goldreich & Kwan 1974; Leung 1978; Stenholm 1980). The alternative approach is a detailed study of an individual source. To infer its parameters, a number of models is constructed and the direct LRT problem is solved for each model. Varying the model parameters, it is possible to find the combination which provides the best agreement between observed and modeled spectra (maps) or their derived parameters, like, e.g., velocity centroids (Walker et al. 1994) or line ratios (van der Tak et al. 2007). Both trial-and-error methods or any sophisticated numerical algorithm for isolating the "best" set of free parameters can be utilized (Keto et al. 2004). This second approach has already been successfully applied in a number of studies, aimed to extract detailed characteristics of pre-stellar and protostellar objects from observed spectra, in particular, their chemical and kinematical structure (e.g., Tafalla et al. 2002, 2004; Keto et al. 2004; Evans et al. 2005; Brinch et al. 2007) as well as to test different star formation theories (e.g. Pavlyuchenkov et al. 2003; Offner et al. 2007).

Following the first approach, efforts of various authors are mainly concentrated toward evolutionary stages later than the prestellar phase. Most cores investigated in detail are closer to the formation of a first hydrostatic core, when the collapse is well-developed and can be described by Shu or Larson-Penston solutions. This interest may be partly caused by the fact that first proofs of infall have been reported for Class 0 objects (Walker et al. 1986; Zhou et al. 1993), in which the collapse has already resulted in the formation of a deeply embedded source. Zhou (1992) considered spectral differences between Shu and Larson-Penston solutions, assuming constant molecular abundances, and identified four line properties, supposedly unique to collapsing cores. Rawlings et al. (1992) combined a dynamical description, based on the Shu model, with a detailed chemical model and identified species with broad line wings, indicative of infall motions. Rawlings & Yates (2001) coupled a similar chemi-

[1] *http://www.sron.rug.nl/~vdtak/radex/radex.php*

cal and dynamical model to a more realistic radiation transfer model, implemented as an approximate Λ-iteration code, and studied the sensitivity of emergent central optically thin and optically thick spectra to various model parameters. The assumption of isothermality, used by Rawlings et al. (1992) and Rawlings & Yates (2001), was relaxed in Tsamis et al. (2008) in application to a "B335-like" Class 0 object. The sensitivity of line profiles in this model to the intensity of the ambient radiation field was studied in Redman et al. (2004). The influence of various parameters on Class 0 central spectra, with a particular emphasis on turbulence and rotation, was also studied by Ward-Thompson & Buckley (2001) under the assumption of flat abundance distributions. The role of high angular resolution in studying such clouds was investigated by Choi (2002). More details about line modeling can be also found in review by Evans (1999).

Large amounts of data have also been accumulated for starless cores, most of which are presumably "prestellar" (e.g., Sohn et al. 2007), together with the theoretical modeling of molecular lines. E.g., Tafalla et al. (2004) investigated the effects of depletion on the line intensity. Lee et al. (2004) studied the evolution of line profiles during core contraction based on the models where the chemical evolution is calculated along with dynamical evolution of the cloud. Pavlyuchenkov et al. (2007) investigated the combined effects of temperature and depletion, and De Vries & Myers (2005) investigated the possibility to use approximate analytical models to extract velocity gradients from the line profiles. In principle, all the mentioned studies of line formation in protostellar objects are also relevant for prestellar cores. However, despite the obvious observational and theoretical progress, the interpretation of the data is still far from being straightforward, as infall and rotation velocities in prestellar cores are both comparable or even smaller than the sound speed. Difficulties in restoring the information about structural, thermal, and kinematic properties are also caused by the lack of relevant methods for molecular line analysis.

In this paper, we systematically study the formation of molecular lines in prestellar cores and present different tools which can be used to analyze the formation of lines in detail. Using the linear molecules CO and HCO^+ as examples, we model their emission by means of non-LTE LRT simulations. The role of hydrogen density, molecular column density, kinetic temperature, infall, and rotation is examined and illustrated in the paper. Such an analysis may form the basis of a more sophisticated interpretation of observational data and can be useful for those who are going to use LRT simulations in their studies or want to get a global view of the factors influencing observed line profiles.

In Section 2 we describe the radiation transfer model used in the paper, introduce parameters to characterize line profiles, and provide some basic considerations on the line formation in prestellar cores. In Section 3 we show how molecular line characteristics depend on hydrogen density, molecular column density, and kinetic temperature for the parameter sample of uniform model clouds. In Section 4 we consider a non-uniform model cloud and study the effects of chemical stratification, contraction and rotation on spectral line maps. In Section 5 we discuss additional problems related to the LRT analysis. Section 6 summarizes the main conclusions of this paper.

2. Notes on Molecular Line Transfer

2.1. Equations of Radiation Transfer

The goal of the LRT simulation is to obtain level populations and to produce appropriate molecular line profiles. For that purpose, one solves a system of equations, describing the radiative transfer (e.g., Peraiah 2001). This system includes the transfer equation itself

$$\frac{dI_\nu}{ds} = -\alpha_\nu I_\nu + j_\nu \tag{1}$$

and a set of balance equations for level populations

$$n_u\left[\sum_{l<u} A_{ul} + \sum_{l\neq u}(B_{ul}\overline{J}_{ul} + C_{ul})\right] = \sum_{l>u} n_l A_{lu} + \sum_{l\neq u} n_l(B_{lu}\overline{J}_{ul} + C_{lu}). \tag{2}$$

Here I_ν is the intensity of radiation, s is the length along the ray, n_u and n_l are level populations, A_{ul} and B_{ul} are the Einstein coefficients; C_{ul} are coefficients of collisional excitation; ul indices specify the transition from the upper level u to the lower level l. Equations (1) and (2) are coupled by the emission and absorption coefficients j_ν and α_ν, respectivelly:

$$j_\nu = \tfrac{h\nu_{ul}}{4\pi} n_u A_{ul} \phi_{ul}(\nu), \tag{3}$$

$$\alpha_\nu = \tfrac{h\nu_{ul}}{4\pi}(n_l B_{lu} - n_u B_{ul})\phi_{ul}(\nu) \tag{4}$$

and by the mean intensity $\overline{J}_{ul}$. The mean intensity is defined as

$$\overline{J}_{ul} = \frac{1}{4\pi}\int\limits_{4\pi} d\Omega \int\limits_0^\infty I_\nu\, \phi_{ul}(\nu) d\nu. \tag{5}$$

where $\phi_{ul}(\nu)$ is the line profile function and Ω is the spatial angle. The line profile function can be expressed as

$$\phi_{ul}(\nu) = \frac{c}{b\nu_{ul}\sqrt{\pi}} \exp\left(-\frac{c^2(\nu - \nu_{ul} - (\vec{v}\,\vec{n})\,\nu_{ul}/c)}{\nu_{ul}^2 b^2}\right) \tag{6}$$

in the approximation of total redistribution over frequencies and a Maxwellian turbulent velocity distribution. Here, ν_{ul} is the central frequency of the transition $u \to l$; $\vec{v}$ is the regular velocity; $\vec{n}$ is unit vector associated with $d\Omega$; and b is a parameter, which is related to the kinetic temperature $T_{\rm kin}$ and the most probable value of the microturbulent velocity $V_{\rm t}$ by the expression

$$b^2 = \sqrt{\frac{2kT_{\rm kin}}{m_{\rm mol}} + V_{\rm t}^2}. \tag{7}$$

The intensity I_ν can be expressed in units of the brightness temperature $T_{\rm B}$ via the Planck equation

$$I_\nu = \frac{2h\nu^3}{c^2}\frac{1}{e^{\frac{h\nu}{kT_{\rm B}}} - 1}, \tag{8}$$

or in the units of radiative temperature $T_{\rm R}$ via the Rayleigh-Jeans approximation with subtracted background radiation

$$T_{\rm R} = \frac{c^2}{2k\nu^2}(I_\nu - I_\nu^{\rm bg}), \tag{9}$$

where $I_\nu^{\rm bg}$ is the intensity of the background radiation with the temperature $T_{\rm bg}$. The radiative temperature $T_{\rm R}$ is commonly used in radio astronomy and we use it throughout this paper.

In order to calculate the emergent profile, one first calculates level populations and then integrates Eq. (1) to get a spectrum, which can be later convolved with a telescope beam, if necessary. For our LRT simulations we use the 2D non-LTE code URAN(IA), developed by Pavlyuchenkov & Shustov (2004). This code partly utilizes the scheme originally proposed and implemented in the publicly available 1D code RATRAN (Hogerheijde & van der Tak 2000). The idea of the method is to solve the system of LRT equations with the Accelerated Λ-Iterations method, where the mean intensity J_ν is calculated with a Monte-Carlo approach.

We focus on pure rotational transitions and restrict ourselves to linear molecules with the simplest level structure (CO, HCO^+) in order to avoid the complexity caused by blends, uncertainties in collisional coefficients, etc. All the molecular data needed for the LRT simulation are taken from the Leiden Molecular Database[2] (Schöier et al. 2005).

To describe and to analyze the results of the simulations, we use two important parameters of the transition, namely, the optical depth τ_ν and the excitation temperature $T_{\rm ex}$. The optical depth is defined as

$$\tau_\nu = \int_{s_0}^{s_1} \alpha_\nu ds, \tag{10}$$

[2] *http://www.strw.leidenuniv.nl/˜moldata/*

where ν is the frequency within the line profile, s_0 and s_1 are near and far edges of the cloud along the ray, respectively, and α_ν is the absorption coefficient. The optical depth determines how opaque the medium is and how effectively different regions are coupled by radiation. The excitation temperature $T_{\rm ex}$ of the transition is defined as

$$\frac{n_l}{n_u} = \frac{g_l}{g_u} \exp\left\{-\frac{h\nu_{ul}}{kT_{\rm ex}}\right\}, \tag{11}$$

where n_l and n_u are populations of levels l and u, and g_l and g_u are their statistical weights. The excitation temperature indicates how close the medium (transition) is to local thermodynamical equilibrium (LTE), when $T_{\rm ex} = T_{\rm kin}$. The excitation temperature and the optical depth can be used to constrain the LRT problem. In the optically thin case the temperature of the emergent radiation $T_{\rm B}$ is proportional to the optical depth and excitation temperature of the transition

$$T_{\rm B} \approx \tau T_{\rm ex}. \tag{12}$$

In the optically thick case

$$T_{\rm B} \approx T_{\rm ex}(\tau = 1), \tag{13}$$

i.e., $T_{\rm B}$ is close to the excitation temperature at $\tau \approx 1$.

2.2. Contribution Chart

Tafalla et al. (2006) implemented the contribution function (CF) as a convenient tool to analyze the relative input of a particular core region to the line profile. They applied it to the study of line formation and chemical differentiation in starless cores, using the frequency-integrated CF. We extend their analysis, taking into account all the velocity channels, and investigate in detail the formation of the entire line profile. The contribution function is defined as

$$F_v(l) = e^{-\tau_v}\left\{1 - e^{-\Delta\tau_v}\right\} S, \tag{14}$$

where τ_v is the optical depth toward the element at distance l, $\Delta\tau_v$ is the optical depth of this element, and S is the source function of the element. The index v indicates that a corresponding value is related to a velocity offset v.

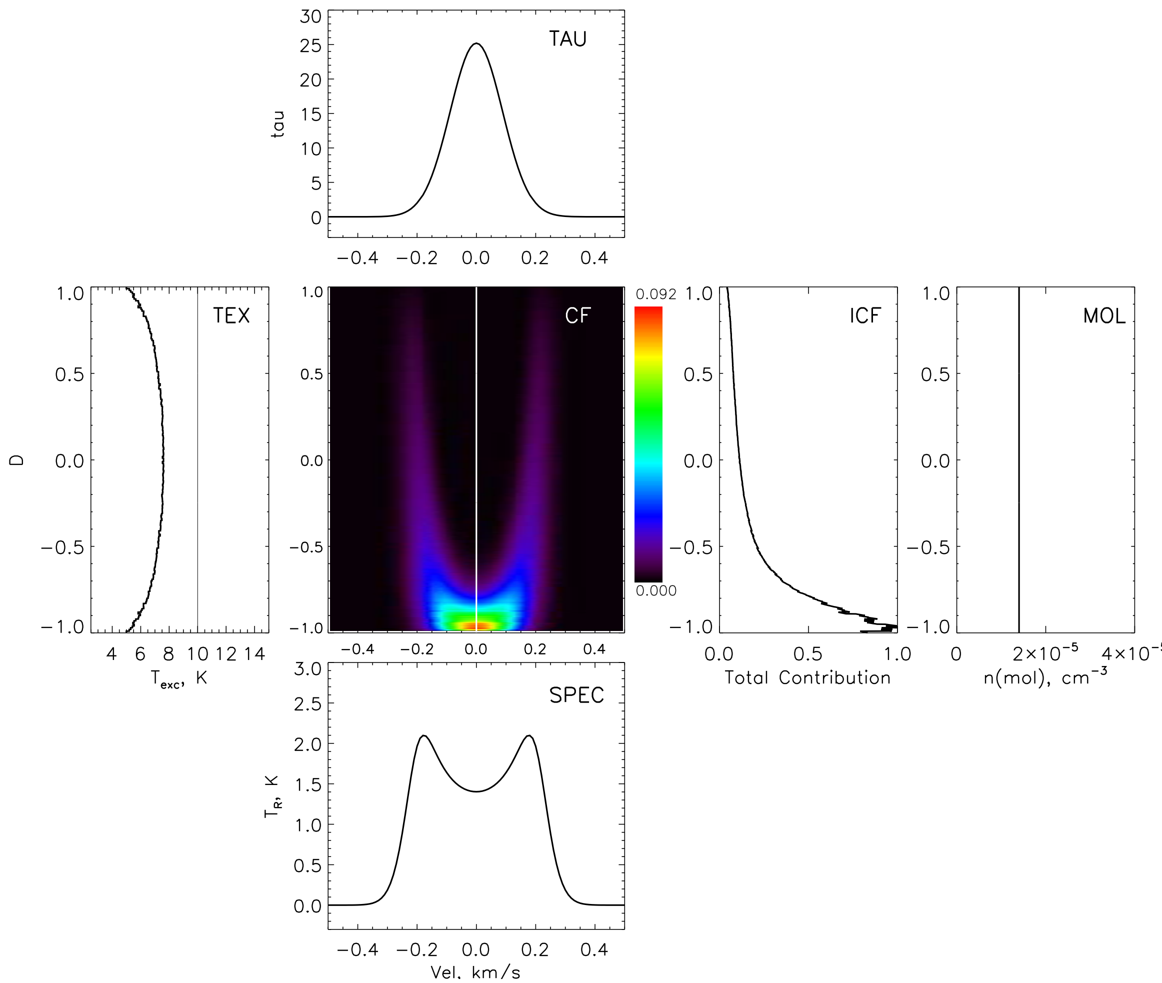

Fig. 1.— Contribution chart for HCO^+(3–2) spectrum from uniform cloud. (SPEC) Emission line profile toward the center of the cloud. (TAU) Spectrum of the optical depth toward the center of the cloud. (TEX) Excitation temperature as a function of position along the ray. The position, D, is given in units of cloud radius. The value $D = -1$ corresponds to the cloud face, while $D = 1$ corresponds to the cloud rear; (MOL) Distribution of the molecular concentration as a function of position. (CF) Contribution function for the given position and velocity offset. The projection of regular velocity onto the line of sight is shown with a white line. (ICF) Contribution function integrated over the velocity.

We find it convenient to combine the contribution function with some other auxiliary plots into a common contribution chart, which is shown in Fig. 1. In this Figure we present results of HCO^+(3–2) line simulations for a static uniform spherically symmetric cloud having $T_{\rm kin} = 10$ K, $n(H_2) = 10^5$ cm^{-3}, $N(HCO^+) = 10^{13}$ cm^{-2} and $V_{\rm turb} = 100$ m/s, which are typical parameters of prestellar cores.

The emergent spectrum for the ray passing through a core center is shown in panel SPEC. Panel TAU contains the corresponding line optical depth. Distributions of excitation temperature and molecular number density along the ray are shown in panels TEX and MOL. The central part of the chart is occupied by a plot depicting the CF for the ray as a function of position and velocity (CF).

From this chart, one readily sees that in this particular example radiation of the line comes almost exclusively from the nearby part of the cloud. Only in wings there is some weak contribution from more remote regions. This is emphasized in panel ICF, where the velocity-integrated CF along the ray is shown. We will see later that in more realistic situations the picture may not be that straightforward.

2.3. Thermalization and Critical Density

Before we start modeling the line profiles under the varios conditions, a brief comment on the conditions in starless cores is in order. There are two primary mechanisms for molecules to be excited in molecular clouds. These mechanisms are collisions with other species (primarily with H_2, He, and e^-) and radiative excitation. The efficiency of the first process depends on gas density and kinetic temperature. The radiative excitation, in turn, depends on the intensity of the ambient radiation field.

To demonstrate the relative importance of collisional and radiative excitation, we consider a simple model of a uniform cloud with temperature $T_{\rm kin}$ and molecular hydrogen density $n(H_2)$, which is illuminated by isotropic blackbody radiation. The temperature of background radiation is set to be $T_{\rm bg} = 2.73$ K (first case) and $T_{\rm bg} = 50$ K (second case), while $T_{\rm kin}$ is varied between 10 K and 100 K. For our analysis, we assume that the cloud is extremely optically thin ($\tau \ll 1$), i.e. we neglect the self-radiation of the cloud to show the effect of radiation and collisions more clearly. We discuss the situation for two molecules with low and large dipole moments, namely, for CO and HCO^+ (note, that their lines, as a rule, are not optically thin in real prestellar cores). Excitation temperatures of CO(2–1) and HCO^+(1–0) as functions of hydrogen density and kinetic temperature are presented in Fig. 2.

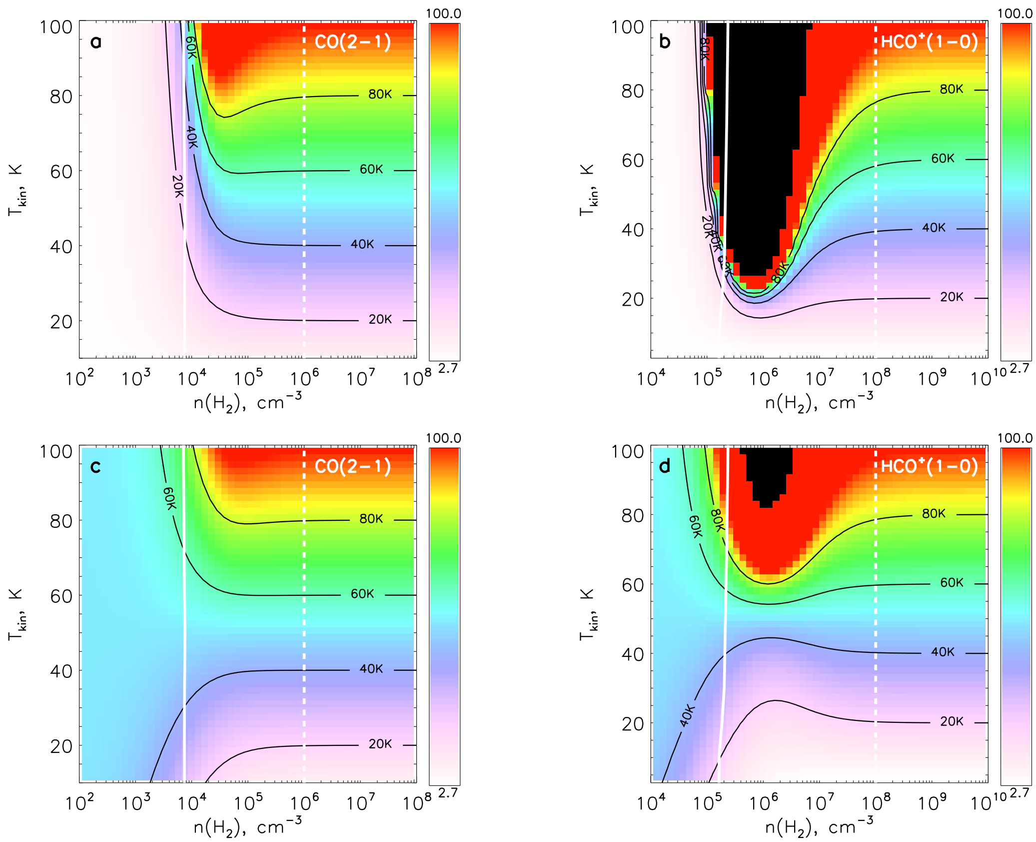

Fig. 2.— Excitation temperature of CO(2–1) and HCO^+(1–0) as a function of hydrogen density and kinetic temperature in the optically thin limit. The temperature of the background radiation is $T_{\rm bg} = 2.73$ K (top row) and 50 K (bottom row). Different colors correspond to different excitation temperatures, as indicated on a scale located to the right of each plot. The black area in the HCO^+(1–0) plots corresponds to negative excitation temperatures, i.e., to an inversion in level populations. The solid white line stands for the critical density $n_{\rm cr}$, see Eq. [15], while the dashed white line corresponds to the thermalization density $n_{\rm th}$.

It can be clearly seen that the map can be divided into three different parts. If the hydrogen density is lower than the so-called "critical density" $n_{\rm cr}$,

$$n_{\rm cr} = \frac{A_{ul}}{\sum_i C_{ui}}, \tag{15}$$

the molecular excitation temperature is determined by the radiation field. In Eq. (15), A_{ul} is the Einstein coefficient and C_{ui} are collisional rates from the upper level u to other low-lying levels i. At densities lower than the critical density, collisions are not effective to excite the molecules. In this region (left part of all plots in Fig. 2) $T_{\rm ex} \approx T_{\rm bg}$ and, thus, does not depend on $T_{\rm kin}$. Note that $n_{\rm cr}$ is different for different transitions. In our case, $n_{\rm cr} \approx 10^4$ cm^{-3} for CO(2–1), and $n_{\rm cr} \approx 10^5$ cm^{-3} for HCO$^+$(1–0). Also, $n_{\rm cr}$ is usually greater for upper transitions of the same molecule.

We also introduce the thermalization density $n_{\rm th}$, as the density, above which collisional transitions define level populations, so that levels are "thermalized", and $T_{\rm ex} \approx T_{\rm kin}$ (right part of all plots in Fig. 2). More precisely, we define $n_{\rm th}$ as a density at which the relative difference between $T_{\rm ex}$ and $T_{\rm kin}$ is 5%.

At intermediate hydrogen densities, $n_{\rm cr} < n({\rm H_2}) < n_{\rm th}$, both collisional and radiative transitions effectively populate and depopulate levels, so that the excitation temperature is equal neither to $T_{\rm kin}$, nor to $T_{\rm bg}$. It can even be negative because of specific ratios between collisional excitation rates. The important point, which we would like to make here, is that these intermediate densities are just typical densities of starless cores. This emphasizes the necessity to use adequate methods for interpretation of observed molecular lines.

2.4. Characterization of Line Profiles

In order to perform a qualitative analysis of line profiles, it is necessary to introduce some values to characterize them. There are different ways to describe numerically a given line profile with a few parameters. In our study we will use the peak intensity $T_{\rm max}$, the total line intensity J (zero moment), the mean velocity $V_{\rm cntr}$ (first moment), the intensity at mean velocity $T_{\rm cntr}$, and the total line width W (second moment). We put a factor $(8\ln 2)$ in the expression for W in order to make W equal to HPBW for Gaussian profiles. In addition, we introduce the relative strength of the self-absorption dip for symmetric profiles, DIP. Definitions for these quantities are given in Table 1 and illustrated in Fig. 3.

Table 1: Parameters of line profiles

Parameter	Definition
Peak intensity, $T_{\rm max}$	$\max\, T_{\rm R}(V)$
Total intensity, J	$\int\limits_{-\infty}^{+\infty} T_{\rm R}(V) dV$
Mean velocity, $V_{\rm cntr}$	$J^{-1} \int\limits_{-\infty}^{+\infty} T_{\rm R}(V) V dV$
Intensity at mean velocity, $T_{\rm cntr}$	$T_{\rm R}(V_{\rm cntr})$
Total line width, W	$\sqrt{(8 \ln 2)\, J^{-1} \int\limits_{-\infty}^{+\infty} (V - V_{\rm cntr})^2 T_{\rm R}(V) dV}$
Self absorption dip, DIP	$(T_{\rm max} - T_{\rm cntr})/T_{\rm max}$

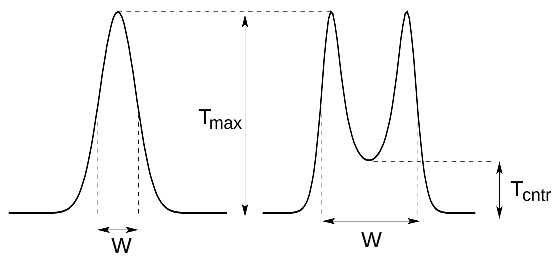

Fig. 3.— Various parameters used to characterize line profiles.

3. Molecular lines from uniform clouds

In the previous section we showed that hydrogen density, gas temperature, and background radiation are all responsible for line excitation. In the optically thin medium, the LRT problem is in some sense local, i.e., the excitation temperature is completely defined by local values of $n(\mathrm{H_2})$, T_{kin}, and by the global radiation field. However, as soon as the total column density of emitting molecules is large enough (i.e., lines become optically thick), the radiation from the entire cloud plays a role in the molecular excitation. Formation of line profiles in the optically thick regime is a complex non-local problem even in the simple case of a static uniform spherically symmetric cloud.

In general, to describe the structure of such a simple cloud one specifies its radius R, temperature, T_{kin}, micro-turbulent velocity, V_{turb}, hydrogen density, $n(\mathrm{H_2})$, and the number density of a molecule, $n(\mathrm{mol})$. However, the solution of the LRT problem depends on R and $n(\mathrm{mol})$ only via their product $R \times n(\mathrm{mol}) = N(\mathrm{mol})$[3].

Therefore, spectra of uniform clouds with different radii and different molecular abundances but with the same molecular column density (other parameters being fixed) should be identical. Values of $n(\mathrm{H_2})$, T_{kin}, and $N(\mathrm{mol})$ are sufficient to get a unique solution of the LRT problem in a uniform cloud (at some velocity v). From the point of view of balance equations, $n(\mathrm{H_2})$ and T_{kin} are needed to calculate collision rates, while $N(\mathrm{mol})$ determines the mean radiation field (in the absence of background radiation). Kinetic temperature and micro-turbulent velocity affect the line width.

To show how basic properties of emergent spectra depend on $n(\mathrm{H_2})$, T_{kin}, and $N(\mathrm{mol})$, we generate a series of models with different parameter sets and perform LRT simulation for each of them. Then, for each model we calculate the spectrum toward the center of the cloud and extract the main line characteristics (see Table 1). As three physical parameters control the line formation in this setup, we vary two of them, keeping the third parameter constant. We present calculated line characteristics as a function of the varied parameters to illustrate their cooperative effects, assuming that all these parameters are independent in the considered ranges. Molecular abundance $X(mol) = n(\mathrm{mol})/n(\mathrm{H_2})$ and temperature T_{kin} are assumed to be uniform over the cloud. For the analysis, we use the $\mathrm{HCO^+}$(3–2) line which is commonly used in observations to probe dense parts of starless cores. *Models in this Section are by no means intended to represent real starless cores. We use them only to demonstrate the main LRT effects.*

---

[3] It is even possible to use $N(\mathrm{mol})/W$ as an independent parameter, where W is the velocity dispersion (see, e.g., Lucas 1974)

3.1. Effects of hydrogen density and molecular column density

In this subsection we consider results of $n(\mathrm{H_2})$ and $N(\mathrm{HCO^+})$ variations at a fixed temperature $T_{\mathrm{kin}} = 10$ K. The cloud is static but has a micro-turbulent velocity V_{turb}=100 m/s, which is a typical value for starless cores. The basic characteristics of an emergent spectrum of $\mathrm{HCO^+}$(3–2) toward the cloud center are presented in Fig. 4.

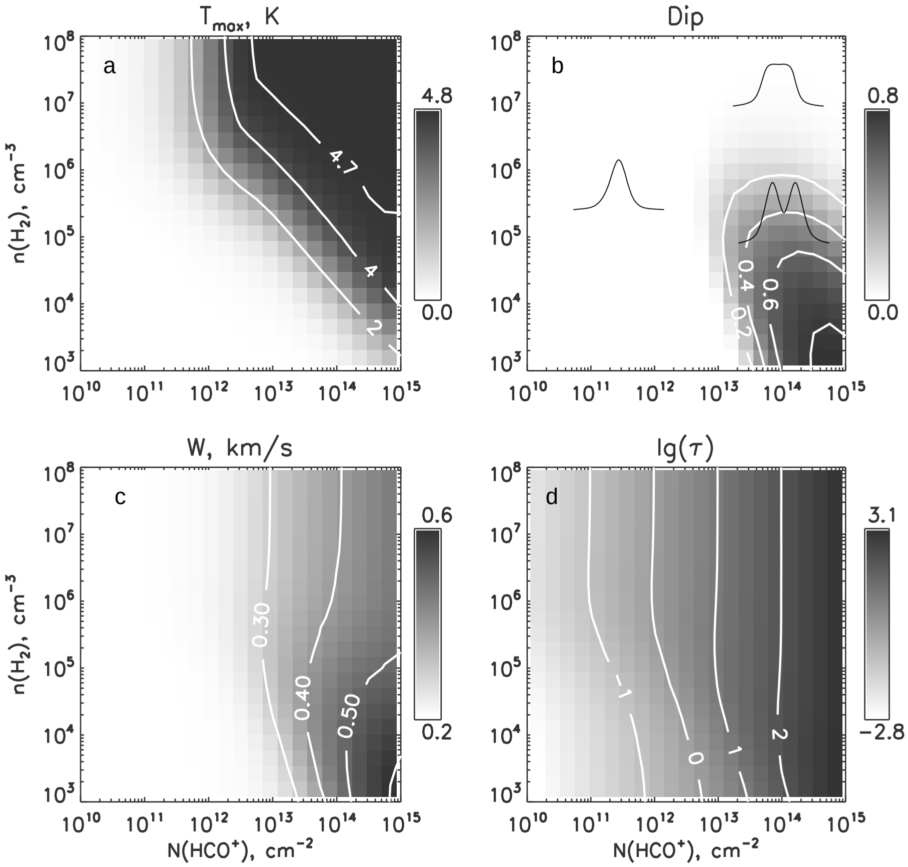

Fig. 4.— Greyscale maps of the line parameters for a uniform cloud. a) Peak intensity, $T_{\max}$, b) relative depth of the self-absorption dip, DIP, c) total line width, W, and d) logarithm of optical depth, $\lg(\tau)$ of the emergent $HCO^+(3–2)$ spectrum as a function of $n(H_2)$ and $N(HCO^+)$. The kinetic temperature is fixed at 10 K.

When both hydrogen density and molecular column density are high (Fig. 4a, top right corner), $T_{\max}$ is close to the LTE value ($T_{\rm R} \approx 4.8$ K for HCO^+(3–2)). At low $n(H_2)$ and/or N(mol) the intensity is also low. However, this plot demonstrates that the common perception of a molecule tracing a specific density is somewhat oversimplified. The comparison of Fig. 4a and Fig. 4b shows that the HCO^+(3–2) profile can be both bright and self-absorbed even if the gas density is much lower than $n_{\rm cr}$, provided the molecular column density is high.

Of course, this situation may not be realistic for HCO^+(3–2) in prestellar cores as at typical HCO^+ abundances of about few times 10^{-9} (Ohishi et al. 1992) the column density of 10^{14} cm^{-2} and the hydrogen density of 10^4 cm^{-3} correspond to a linear extent of about 3 pc. But, it can be relevant for other molecules and/or transitions, e.g. for CO(3–2). With a column density $N({\rm CO}) = 10^{17}$ cm^{-2} (which corresponds to an optical depth of about 100), density $n(H_2) = 10^3$ cm^{-3} (below critical), and molecular abundance $X({\rm CO}) = 10^{-4}$, the linear extent of the cloud is about 0.3 pc, which is comparable to typical sizes of prestellar cores.

On top right panel of Fig. 4, the relative strength of the self-absorption dip is shown. As long as DIP = 0, the profile is single-peaked, otherwise it is double-peaked. The dip in HCO^+(3–2) line appears when the molecular column density is larger than 10^{13} cm^{-2}. This corresponds to an optical depth $\approx$1, and a hydrogen density $n(H_2) \leq n_{\rm cr}$. If the density is greater than the critical density, the line has a single peak even at very high HCO^+ column density. The self-absorption profile forms when a gradient in the excitation temperature is present. But at high density the excitation temperature is equal to the kinetic temperature over the whole cloud (which is assumed to be uniform). Thus, in such a situation we obtain a flat-top profile instead of a self-absorbed profile.

In the bottom panels of Fig. 4, the total line width of the spectra and the optical depth are shown as functions of $n(H_2)$ and N(mol). Both parameters are mostly determined by the molecular column density and only weakly depend on gas density.

We consider a broad range of HCO^+ column densities (five orders of magnitude), with lower values being not typical for prestellar cores. Our reason is two-fold. First, we intend to show the effects of LRT in general. Second, the presented plots can be relevant for the isotopomers of HCO^+, e.g. for $H^{13}CO^+$ and $HC^{18}O^+$ which have similar excitation parameters but smaller abundances (defined by both isotopic ratios and isotope-dependent chemistry).

3.2. Effects of kinetic temperature and hydrogen density

In Fig. 5 we show the combined effect of temperature and hydrogen density variations, keeping the molecular column density constant. To show the complexity of the LRT effects, we explore the case of a moderate optical depth, which corresponds to a representative value of $N(\mathrm{HCO}^+) = 10^{13}$ cm^{-2}, as follows from the previous subsection. This value is close to that inferred for the CB17 globule in Pavlyuchenkov et al. (2006). To test the sensitivity of the considered parameters, we vary the temperature in a range, which is wider than is inferred for starless cores, however, all the patterns described below are seen at $T_{\mathrm{kin}} < 20$ K.

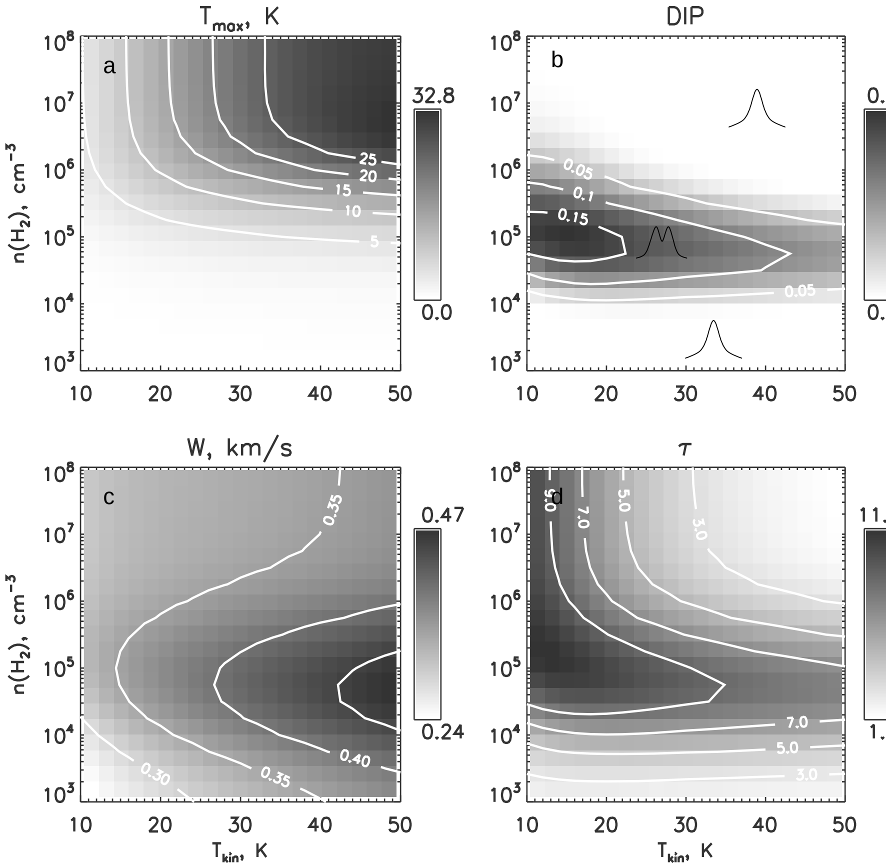

Fig. 5.— Line parameters as functions of $n(\mathrm{H_2})$ and T_{kin} at a fixed column density $N(\mathrm{HCO^+}) = 10^{13}$ cm^{-2} for a uniform cloud. a) Peak intensity, T_{max}, b) relative depth of the self-absorption dip, DIP, c) total line width, W, and d) optical depth, τ, of the emergent $\mathrm{HCO^+}$(3–2) spectrum are shown.

The increase in temperature as well as the increase in hydrogen density leads to an increase of the line intensity. At 10 K, the self-absorption dip only appears at densities between 10^4 and 10^6 cm^{-3}. At densities below 10^4 cm^{-3} collisional excitation is too slow to populate levels of the transition, and the optical depth is also correspondingly low. At larger densities ($> 10^6$) levels higher than 3 are populated more efficiently, while lower levels are thermalized. Because of this fact, population of lower levels decreases, which results in a low optical depth for densities above 10^6 cm^{-3}. The line width is sensitive to the self-absorption dip and thus has its maximum at densities between 10^4 and 10^6 cm^{-3}. When temperatures are higher, the density range, at which the dip appears, gets narrower, and the dip itself becomes less pronounced, while the line becomes wider, and its optical depth decreases.

Even though we consider just one particular molecule and particular transition, the same diagrams can be obtained for other molecules and transitions. In essence, the diagrams for linear molecules (for the same transitions) look similar. The difference is that features of the diagrams are shifted along the corresponding axes reflecting different critical densities and different column densities per unit optical depth. Such diagrams for more complicated models can be used to illustrate the main non-LTE effects of the line formation process and to derive parameters of prestellar cores from the observed spectra.

4. Molecular line formation in starless cores

Even in uniform clouds and in the absence of regular velocity field, line shapes can be quite different from simple gaussians, having self-absorption dips or flat tops due to thermalization (see above). Of course, when regular velocity fields and chemical differentiation are taken into account, line profiles become even more diverse, which further complicates their analysis. In this Section we consider the formation of the HCO^+(1–0) line in the presence of chemical stratification and regular motions, using a simple "chemo-dynamical" model, where the chemical evolution is calculated along with the dynamical evolution of the core.

4.1. Model of starless core

We assume that a starless core is spherically symmetric with the density distribution given by $n(r) = n_0/(1+(r/r_0)^p)$, where $p = 2.4$, $r_0 = 2800$ AU, $n_0 = 1.35\times10^6$ cm^{-3}. Parameters are chosen to represent the L1544 core (Tafalla et al. 2004). To calculate the chemical and kinematic structure of a starless core, we use the model described in Pavlyuchenkov et al. (2006).

We consider models of a static core, collapsing core, and rotating core. To quantify collapse and rotation velocities, we assume that the model core forms over a time $t_0 = 0.8$ Myr as a result of contraction from an uniform initial configuration with density $n_{\rm ini} = 5 \cdot 10^3$ cm^{-3} and rotation velocity at the core edge $V_0 = 100$ m s^{-1}. The micro-turbulent velocity is 100 m s^{-1} in the static model and 50 m s^{-1} in the non-static models. Molecular abundances are calculated with the same chemical model as described in Pavlyuchenkov et al. (2006). Briefly, it is a time-dependent chemical model which includes gas-phase reactions as well as the freezing-out of molecules onto dust grains and their desorption back to the gas-phase. Surface reactions are not taken into account. Species stick to dust grains with the probability of 0.3 for all components except for H_2 and He, for which zero sticking is assumed. We calculate the sticking probability for atomic hydrogen according to Hollenbach & McKee (1979). Three desorption mechanisms are taken into account, which are thermal desorption, photodesorption, and cosmic ray induced desorption. It is assumed that a cosmic ray particle impulsively heats a dust grain to a peak temperature $T_{\rm crp}$, which is close to 70 K for cold 0.1μm silicate grain. Data from Léger et al. (1985) are used to approximate the dependence of $T_{\rm crp}$ on the initial dust temperature (Semenov et al. 2004). Gas-phase reactions are taken from the UMIST 95 ratefile (Millar et al. 1997). We consider the evolution of species containing H, He, C, N, O, Mg, Na, Fe, S, and Si atoms.

Kinetic temperature is assumed to be 9 K. The core is subject to an external UV field with the intensity, G, measured in units of the mean interstellar field (Draine 1978), and to cosmic rays, which ionize molecular hydrogen with the rate ζ. The assumed distance to the core is 140 pc as believed to be relevant for cores in Taurus cloud complex (which in fact maybe closer; see note in Goldsmith et al. (2008)). Using these parameters we perform LRT simulations and produce "ideal" (non-convolved) spectral maps and contribution charts for the HCO^+(1–0) line.

To illustrate the importance of the cosmic ray (CR) ionization rate and ultraviolet (UV) radiation intensity for the chemical structure of the core in Fig. 6 we present abundance profiles for HCO^+ molecules calculated with $G = 0.01$ and 1.0 and $\zeta = 10^{-18}$ s^{-1} and 10^{-16} s^{-1} at $t = 0.8$ Myr.

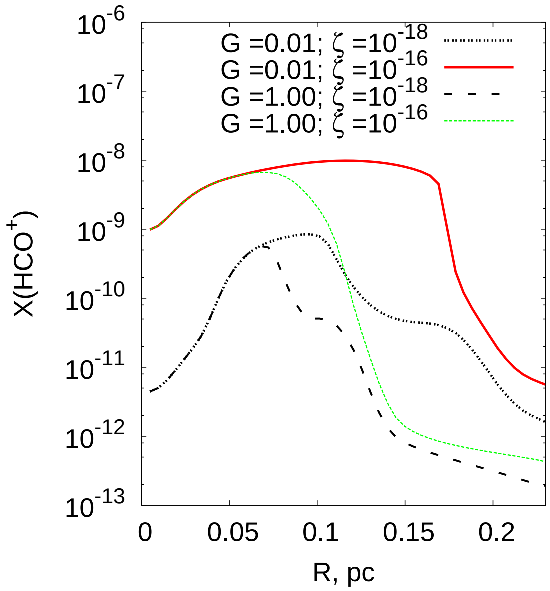

Fig. 6.— Distribution of the HCO^+ relative abundances in the prestellar core model for the different parameters of UV radiation and CR flux.

The relative abundance of HCO^+ strongly depends on both parameters and varies up to a few orders of magnitude. The strong UV radiation destroys molecules in the envelope, while enhanced CR flux prevents molecules from sticking to dust grains (via CR-induced desorption) and enhances HCO^+ abundance over the whole cloud.

4.2. Static core

We first assume that the core is static, i.e., both infall and rotation velocities are zero. The calculated spectral map and the contribution chart for the central spectrum are shown in Fig. 7 for the case when $G = 0.1$ and $\zeta = 10^{-18}$ s^{-1}.

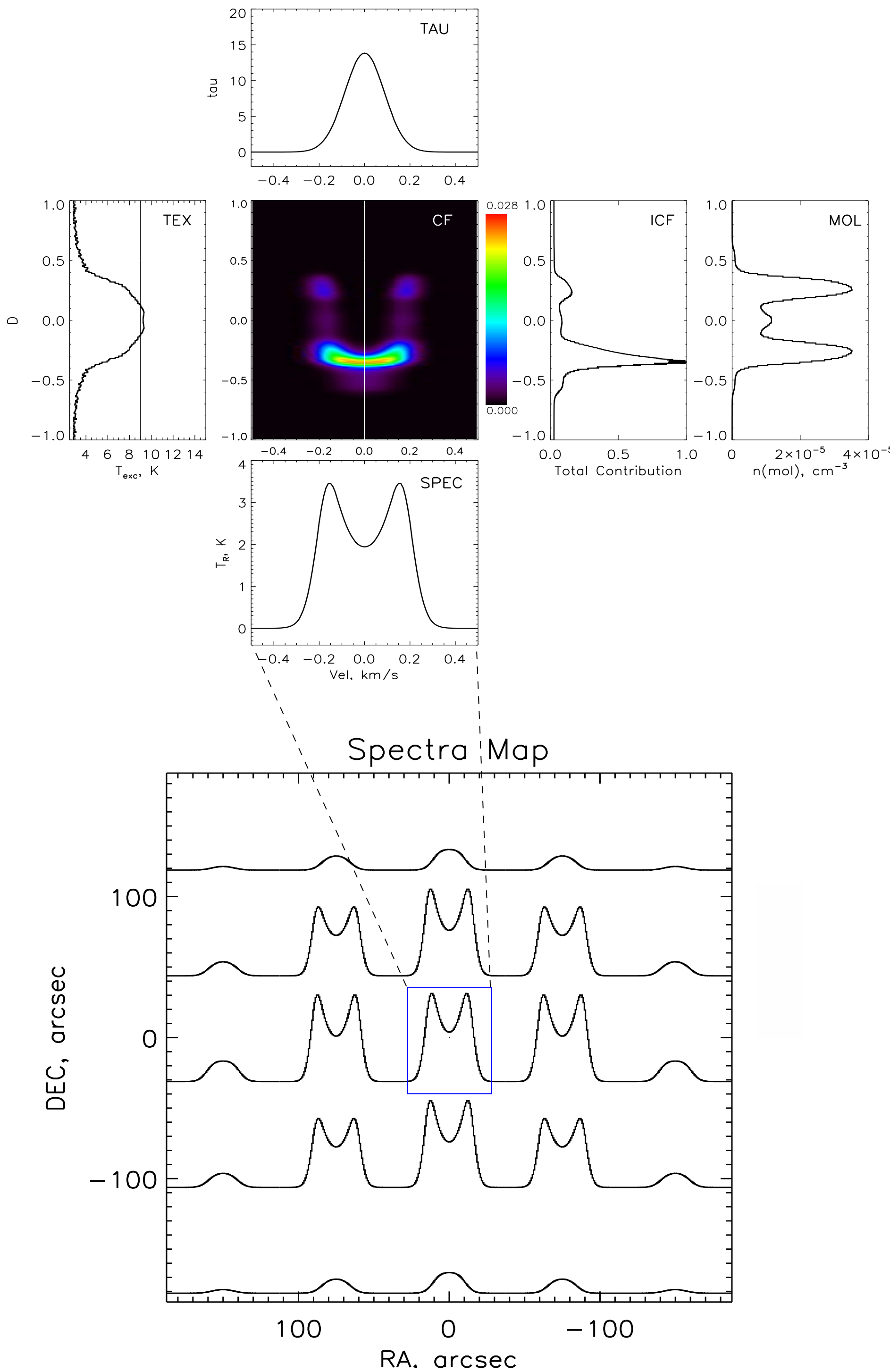

Fig. 7.— Top: Contribution chart for the central spectrum of the non-uniform static core. Bottom: Spectral map of HCO^+(1–0) for the same core.

The contribution chart demonstrates all the aspects of $HCO^+(1–0)$ line formation. In the inner part of the core the excitation temperature $T_{\rm ex}$ is nearly equal to the kinetic temperature while in the envelope it decreases with radius (TEX). This is mainly because of the lower density in the envelope, so that collisions are not effective enough to excite the level populations. The molecular density distribution is not uniform but has a maximum at $R/R_0 = 0.2$ (MOL). In the inner part the core molecules are depleted onto the dust grains. The optical depth in the line center is about 20, i.e., the line is optically thick (TAU). From the chart, it can be seen that emission in the line center comes from the outer part of the core where the excitation temperature is relatively low. The emission in blue and red peaks comes mainly from inside, where the excitation temperature is higher. This results in the double peaked profile. At the same time, the very center of the core does not contribute to the $HCO^+(1–0)$ profile even in line wings because of molecular depletion.

4.2.1. Uncertainties of the chemical structure

A non-uniform chemical structure of starless cores is of crucial importance for the interpretation of observed spectral maps. A particular starless core may look very different in lines of various molecules just because of the different molecular abundance distributions (Tafalla et al. 2002). In general, current models of starless cores, which include chemical and micro-physical processes (e.g., depletion and desorption of molecules on dust grains), allow us to understand *qualitatively* distributions of simple molecules like CO, CS, HCO^+, and N_2H^+ (see, e.g., Bergin & Tafalla 2007; Aikawa et al. 2008). However, it is still difficult to use such models for the *quantitative* analysis, mainly because of two reasons. First, rates of many chemical and physical processes, involved in determining the abundance gradients, are still very uncertain. Here we refer to the papers by Vasyunin et al. (2004) and Wakelam et al. (2006) where the uncertainties of chemical reaction rates are studied. Second, external physical conditions such as intensity of the CR and UV radiation fields, are often not well constrained, but they strongly affect the core chemical structure (see, e.g., Farquhar et al. 1994; Pavlyuchenkov et al. 2006).

Here we want to illustrate the influence of the G and ζ values on the emergent spectra. We consider a range of "L1544-like" models, but varying G from 0.01 to 1 and ζ from 10^{-18} s^{-1} to 10^{-16} s^{-1}. The resulting difference in abundances affects both the intensity and the relative strength of the self-absorption dip (Fig. 8).

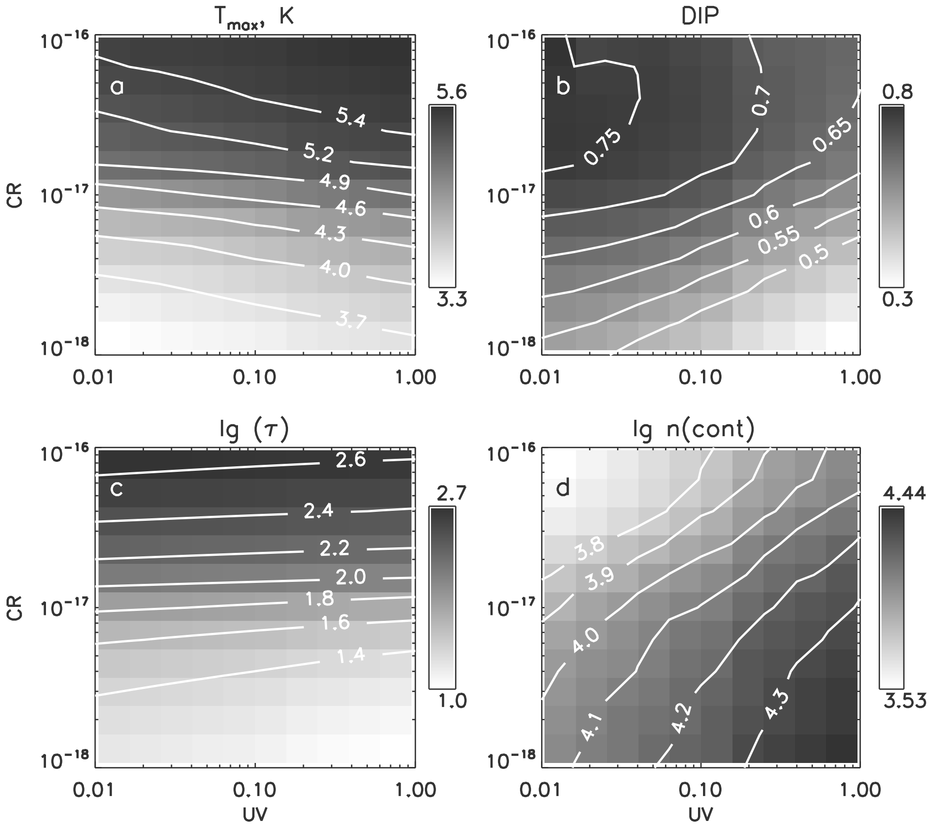

Fig. 8.— Results of the variation of the UV and CR radiation fields for a non-uniform model of a prestellar core. a) Peak intensity, $T_{\rm max}$, b) relative strength of the self-absorption dip, DIP, c) the logarithm of optical depth, lg (τ), and d) the logarithm of contributing density $\lg n(\mathrm{cont})$, (see text) of the line formation for HCO^+(1–0) are shown as functions of G and ζ.

In the bottom right panel we show the density of the line formation, or "contributing density", which we define as the density where the integrated contribution function has a maximum (Fig. 7-ICF). This density approximately indicates which densities are actually "traced" by the considered transition. The contributing density depends on the UV and CR values and can be even smaller than the critical density (cf. Fig. 2). In the adopted parameter space the optical depth of the HCO^+(1–0) transition varies from 10 to 1000.

From the point of view of the line intensity and its optical depth, ζ seems to be more important than G. The reason is chemistry. In the considered parameter space, $T_{\rm max}$ and τ almost do not depend on the UV field intensity, because, when G increases, the maximum of the absolute HCO^+ abundance just moves deeper into core, without changing the column density much. On the other hand, an increase in ζ affects the entire core, enhancing the gas-phase molecule abundance and the column density.

As can be seen from Fig. 4d, the optical depth depends strongly on the column density and is almost independent on gas density (i.e., excitation conditions). This is reflected in Fig. 8c. Peak intensity and the depth of the self-absorption dip depend both on molecular column density and H_2 volume density (Fig. 4a,b). Thus, the corresponding plots in Fig. 8a,b have a more "diagonal" appearance. The dip gets deeper as the UV intensity decreases, because at lower G the maximum HCO^+ abundance occurs closer to the core edge, i.e., at smaller densities. In other words, when G is low, HCO^+(1–0) traces lower densities (Fig. 8d).

It must be noted that the description used in this subsection is somewhat simplified in the sense that it does not take into account the temperature gradient which may appear due to enhanced UV irradiation and/or CR flux. Even though these small temperature variations are of minor importance for chemistry, they do affect the excitation conditions and, thus, further complicate the situation.

4.3. Collapsing core

The next step is to abandon the assumption of zero regular velocity in the core. First, we assume that the core is contracting, with a maximum infall velocity of about 50 m/s. The corresponding spectral map is shown in Fig. 9 for the case with $G = 0.1$ and $\zeta = 10^{-18}$ s^{-1}.

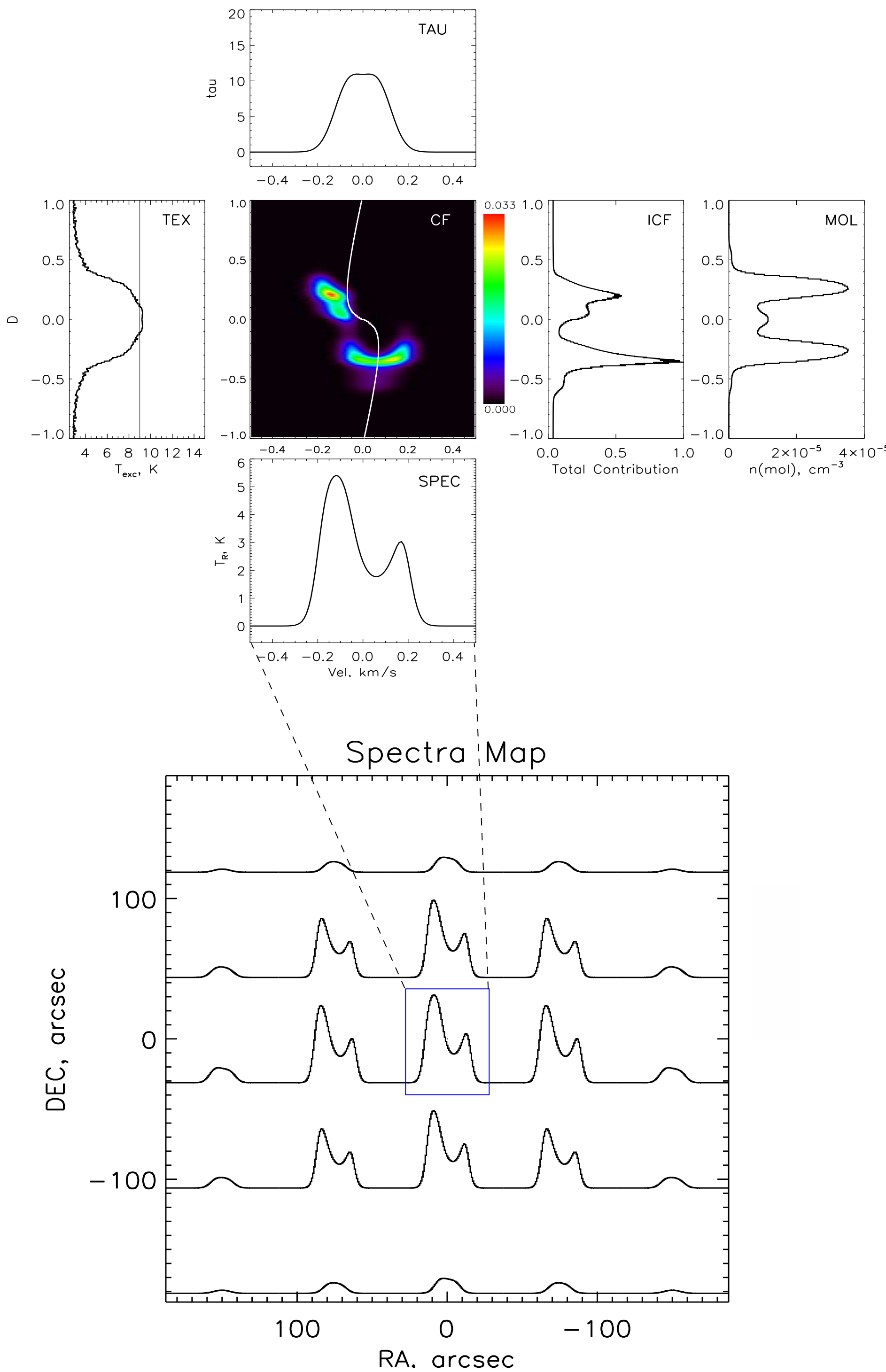

Fig. 9.— Contribution chart for HCO^+(1–0) emission from the collapsing core with $G = 0.1$ and $\zeta = 10^{-18}$ s^{-1}. Because of strong depletion, the line peaks mainly form in the outer parts of the core, but there is still some contribution of the core center in the blue peak. Projection of regular velocity onto the line of sight is shown with a white line.

In contrast to the static model, line profiles show the classical infall asymmetry, with the blue peak dominating over the red peak. The map itself is symmetric relative to the center. The combination of factors behind the line profile asymmetry is well seen on the chart. The contribution chart for the central spectrum (Fig. 9) has a complex appearance, which, in general, follows the projected velocity (white curve in Fig. 9). There is a common perception that optically thick lines trace outer parts of the source. However, as we see from the chart in Fig. 9, in general, the line profile includes information about different parts of the cloud. The integrated contribution function (Fig. 9-ICF) shows that both near and far parts of the core participate in the formation of the central spectrum. As in the static case (Fig. 7), the emission around the dip (at zero velocity) and in the red peak comes from the envelope part closest to the observer. However, this region contributes some emission in the blue peak as well. The most of the emission in the blue peak comes from the rear part of the model core (a hallmark of the infall asymmetry) and also from its center. The gap between the near and rear parts of the contribution function (Fig. 9-CF) at negative velocities is caused by depletion of HCO^+ in the core center.

Self-absorption spectra toward centers of some prestellar cores (e.g. Lee et al. 1999, 2001) are dominated by red peaks, as if the corresponding core is expanding. The asymmetry of the line profile in a particular core can also be caused by an outflow powered by an unseen central object (protostar). In addition, spectral maps of some cores (e.g. Lada et al. 2003) indicate that their kinematics cannot be described as pure contraction, expansion and/or rotation. Keto et al. (2006) suggested that the velocity field in these prestellar cores can be reproduced by a model of an oscillating pressure-bounded, thermally-supported object.

If we, for the purpose of discussion, consider a model of an expanding core by changing the velocity sign, we end up with a spectral map and contribution chart for the central spectrum, which are just mirror reflections of the same plots for the model of contracting core but with the opposite asymmetry. In general, a detailed dynamical model is needed to quantify such motions.

4.4. Rotating core

Now, we assume that the core does not collapse, but rotate with the axis being perpendicular to the line of sight. The corresponding spectral map and the contribution chart for HCO^+(1–0) are presented in Fig. 10. The line profiles are asymmetric everywhere in the map except for the projection of the rotation axis. To the left of this axis, profiles are blue-dominated and blue-shifted along the velocity, while to its right they are red-dominated and red-shifted. The map is symmetric with respect to the projection of the rotation axis.

As in the case of the contracting core, the appearance of the contribution function follows the projected velocity.

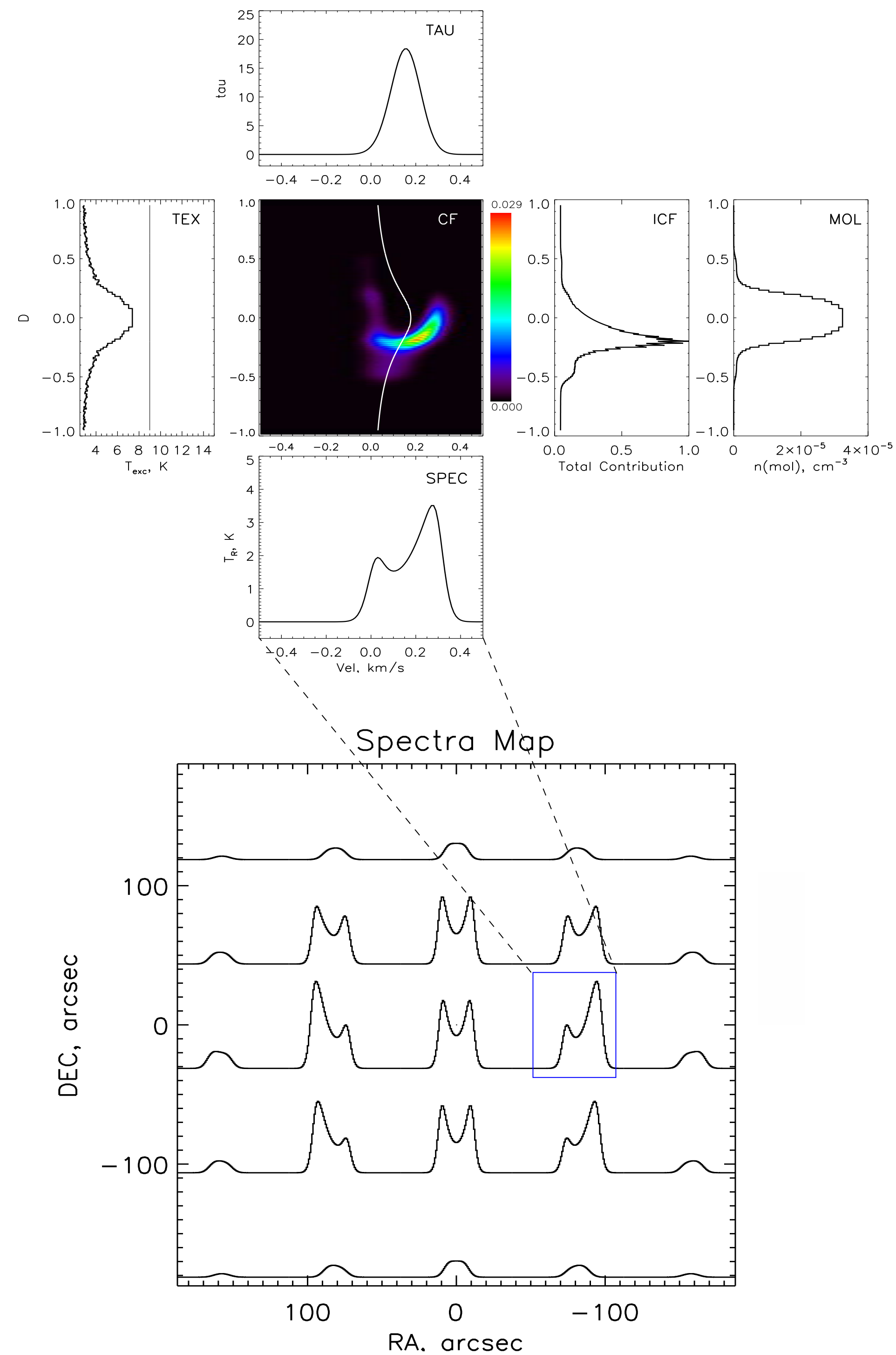

Fig. 10.— Contribution chart for HCO^+(1–0) emission from the rotating core. Projection of the rotation velocity onto the line of sight is shown with a white line.

Comparing lines from contracting and rotating models, we see that they produce very similar profiles in some off-central positions. Therefore, in order to distinguish between the models it is necessary to analyze the complete spectral map, not just the central or single off-central spectrum. Moreover, in order to extract the information about kinematics of the cloud it is of a great importance to analyze simultaneously spectral maps for different transitions (optically thin and optically thick) and different molecules.

4.5. Collapsing and Rotating core

Finally, let us assume the more realistic case, i.e. that the core is collapsing and rotating at the same time. The corresponding spectral line map and the contribution chart for HCO^+(1–0) and $i = 90°$ are presented in Fig. 11. The spectra map is no longer symmetric, neither with respect to the center (as in the case of a purely contracting core), nor with respect to the projection of the rotation axis (as in the case of pure rotation). On the left side of the map, the effects of infall and rotation are coherent and profiles are strongly blue-dominated. On the right side of the map, infall and rotation tend to produce opposide line asymmetries (see Fig. 9–10) and their net result is the formation of nearly symmetric line profiles. To the left of the rotation axis, profiles are blue-shifted, while to its right they are red-shifted, as in the case of pure rotation.

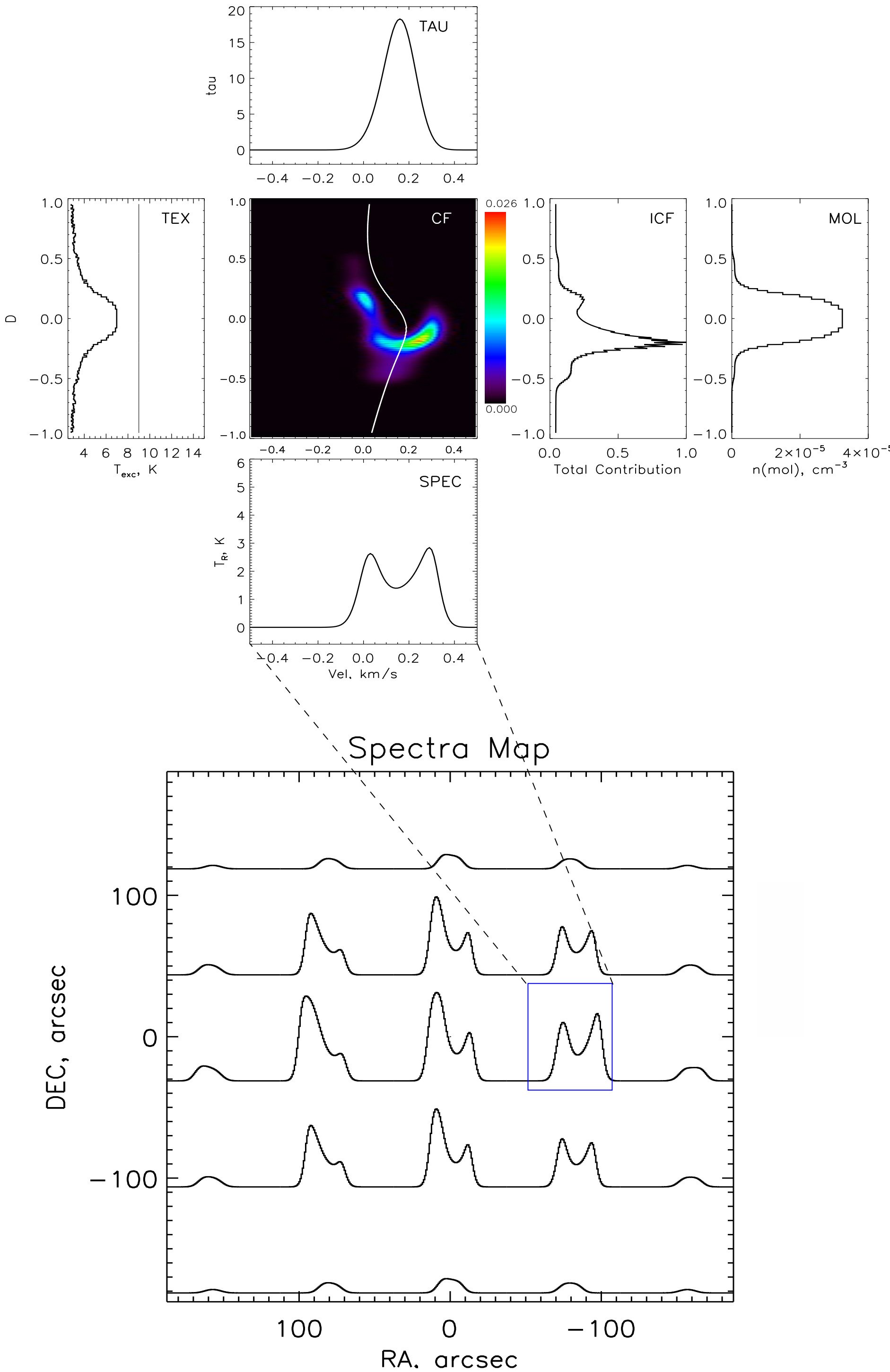

Fig. 11.— Contribution chart for the $HCO^+(1\text{–}0)$ emission from a collapsing and rotating core. The projection of the regular velocity onto the line of sight is shown with a white line.

Combination of collapse and rotation allows to reproduce the spectral features observed in a number of molecular cores. In particular, Pavlyuchenkov et al. (2006) used a similar model for the CB17 prestellar core and derived the infall and rotation velocity by fitting the maps of optically thin and optically thick lines simulteneously. The presence of both rotation and infall is also seen in the L1544 core (Ohashi et al. 1999; Williams et al. 2006). To distinguish between rotation and infall it is also useful to use the first-moment maps, (e.g. Walker et al. 1994; Chen et al. 2007).

5. Discussion

Starless cores arguably represent the simplest configuration among all stages of the formation of a low-mass star. Despite this simplicity, the interpretation of observed spectra is not straightforward, especially, in terms of kinematics, because regular motions in these objects have velocities which are comparable to or even less than the sound speed.

Above, we have given some examples of molecular line formation in static and dynamic cores, demonstrating how line profiles are influenced by gas density and temperature, molecular abundance, presence of regular motions, and external parameters which drive the chemical evolution. Contribution charts show clearly that any optically thick line, generally speaking, does not represent some specific part of the core but rather combines contributions from different regions. Incidentally, this is what makes it possible to use optically thick lines as a diagnostic for core-wide kinematics. On the other hand, while the contribution function in general follows the regular velocity profile, emission at a given velocity is not unambiguously related to a region which moves with this velocity, bearing information from other regions as well because of finite microturbulent line broadening.

There are some other potential complications which are not accounted for in the present paper. In particular, in the models presented above, the gas temperature is assumed to be uniform over the core. In reality, the thermal structure of starless cores can be more complex. Following the theoretical considerations, the gas temperature is a result of heating by cosmic rays, photoelectric heating, collisional exchange with dust, and cooling by atomic and molecular lines. The dust temperature, in turn, is mostly controlled by external radiation and expected to rise from inside ($\sim 5-7$ K) to outside (~ 15 K) (see e.g. Zucconi et al. 2001; Evans et al. 2001; Young et al. 2004). Cooling by molecular and atomic lines depends on the abundance of key species, like CO, C and C^+ (Goldsmith 2001). Thus, in order to estimate the gas temperature distribution one needs to model the chemical structure, line radiative transfer, and the energy exchange between gas and dust. Keto & Caselli (2008) showed that the thermal structure of starless cores may differ depending on their central density. For cores with high central density ($n(\mathrm{H_2}) > 10^5$ cm^{-3}), the temperature rises from inside to outside, while for less dense cores the temperature distribution is more uniform, which seems to be supported by observations of several prestellar cores. As shown by Pavlyuchenkov et al. (2007) over-simplified thermal models may lead to wrong interpretations of line data. Thus, the thermal structure of the starless cores should be considered in the LRT simulations. In fact, the sensitivity of CO lines to the gas temperature in the envelope makes it possible to use these lines to constrain the UV part of the radiation field, while the dust RT modeling allows to estimate the overall level of the interstellar radiation field, (see Evans et al. 2005).

From the observational side, there is a convolution problem which is related to the finite resolution of radio-telescopes. If the telescope beam is comparable to the angular size of an object then different regions contribute to the emergent line profile which makes derivation of source parameters even more difficult and often ambiguous.

There are also some uncertainties which are related to the LRT problem itself. One of them is the commonly used assumption of the full frequency redistribution (FFR) over the line profile which dramatically simplifies equations of the LRT (e.g., the source function does not depend on frequency). However, this assumption may not be valid in low density regions where collisions are not frequent enough to redistribute the absorbed energy. As a result, the line formation may proceed in a way between two extreme modes, namely, between FFR and coherent scattering. In the latter case, lines would not have any self-absorption dips (but shapes can still be complex because of the regular velocity).

Another commonly used approach is to simplify the non-regular (turbulent) velocity field in cores by introducing the micro-turbulence velocity (Eq. [7]). Such representation of the real (unknown) velocity field by the combination of the regular and microturbulent velocities also may lead to misinterpretations. For instance, line asymmetry can be considered as an evidence of infall (outflow), being actually a reflection of a complex kinematic structure due to turbulence or oscillations. Moreover, even if we are not interested in line shapes, the microturbulent approach can fail in reproducing line intensities. As shown by, e.g., Hegmann & Kegel (2000), the turbulent structure of prestellar cores can be rather represented by meso-turbulence which again requires the modification of the radiative transfer equation.

6. Conclusions

In this paper we analyze molecular line formation at conditions typical of starless cores. In particular, we show the effect of density, molecular column density, and temperature on line parameters for a sample of uniform clouds. We also consider non-uniform models and show the effect of the chemical differentiation, collapse and rotation on the molecular spectral maps. We present a chart of line formation which may serve as valuable tool for understanding results of LRT simulations. This chart clearly demonstrates which parts of the model core contribute to the line profile at each velocity.

We would like to make the following conclusions:

- Densities in starless cores fall into the range where level populations are neither radiatively, nor collisionally dominated.
- Large column densities do not necessarily lead to the appearance of self-absorption dips.
- When the column density is fixed, a specific line can be optically thick only in a range of densities, being optically thin at densities both below and above this range.
- The density which is "traced" by some transition depends on external factors (UV field and CR ionization), which shape the molecular distribution. In particular, the "traced" density can be lower than the critical density.
- Rotation and infall may produce very similar spectra and in general can only be distinguished by spectral mapping.

We are grateful to Ted Bergin, Michiel Hogerheijde, Kees Dullemond and Juergen Steinacker for useful discussions. We also thank the referee Neal J. Evans II, for valuable suggestions and comments. This research has made use of NASA's Astrophysics Data System. DW, and BS are supported by the RFBR grant 07-02-01031.

REFERENCES

Aikawa, Y., Wakelam, V., Garrod, R. T., & Herbst, E. 2008, ApJ, 674, 984

Bergin, E. A., & Tafalla, M. 2007, ARA&A, 45, 339

Brinch, C., Crapsi, A., Hogerheijde, M. R., & Jørgensen, J. K. 2007, A&A, 461, 1037

Chen, X., Launhardt, R., & Henning, T. 2007, ApJ, 669, 1058

Choi, M. 2002, ApJ, 575, 900

Crapsi, A., Caselli, P., Walmsley, M. C., & Tafalla, M. 2007, A&A, 470, 221

De Vries, C. H., & Myers, P. C. 2005, ApJ, 620, 800

di Francesco, J., Evans, N. J., II, Caselli, P., Myers, P. C., Shirley, Y., Aikawa, Y., & Tafalla, M. 2007, Protostars and Planets V, 17; B. Reipurth, D. Jewitt, and K. Keil (eds.), University of Arizona Press, Tucson, 951 pp., 2007., p.17-32

Draine, B. T. 1978 ApJS, 36, 595

Evans, N. J., II 1999, ARA&A, 37, 311

Evans, N. J., II, Rawlings, J. M. C., Shirley, Y. L., & Mundy, L. G. 2001, ApJ, 557,

Evans, N. J., II, Lee, J.-E., Rawlings, J. M. C., & Choi, M. 2005, ApJ, 626, 919

Farquhar, P. R. A., Millar, T. J., & Herbst, E. 1994, MNRAS, 269, 641

Goldreich, P., & Kwan, J. 1974, ApJ, 189, 441

Goldsmith, P. F. 2001, ApJ, 557, 736

Goldsmith,P. F., Heyer,M., Narayanan,G., Snell,R., Li,D., & Brunt,Ch. 2008, ApJ, 680, 428

Hegmann, M., & Kegel, W. H. 2000, A&A, 359, 405

Hogerheijde, M. R., & van der Tak, F. F. S. 2000, A&A, 362, 697

Hollenbach, D., & McKee, Ch. F. 1979, ApJS, 41, 555

Keto, E., Rybicki, G. B., Bergin, E. A., & Plume, R. 2004, ApJ, 613, 355

Keto, E., Broderick, A. E., Lada, C. J., & Narayan, R. 2006, ApJ, 652, 1366

Keto, E., & Caselli, P. 2008, ApJ, in press.

Mac Low, M.-M., & Klessen, R. S. 2004, Reviews of Modern Physics, 76, 125

Lada, C. J., Bergin, E. A., Alves, J. F., & Huard, T. L. 2003, ApJ, 586, 286

Lee, C. W., Myers, P. C., & Tafalla, M. 1999, ApJ, 526, 788

Lee, C. W., Myers, P. C., & Tafalla, M. 2001, ApJS, 136, 703

Lee, J.-E., Bergin, E. A., & Evans, N. J., II 2004, ApJ, 617, 360

Leung, C. M. 1978, ApJ, 225, 427

Léger, A., Jura, M., Omont, A. 1985, A&A, 144, 147

Lucas, R. 1974, A&A, 36, 465

Millar, T. J., Farquhar, P. R. A., & Willacy, K. 1997, A&AS, 121, 139

Myers, P. C. 1999, The Physics and Chemistry of the Interstellar Medium, 227, Proceedings of the 3rd Cologne-Zermatt Symposium, Eds.: V. Ossenkopf, J. Stutzki, and G. Winnewisser

Offner, S. S. R., Krumholz, M. R., Klein, R. I., & McKee, C. F. 2007, ArXiv e-prints, 712, arXiv:0712.3053

Ohashi, N., Lee, S. W., Wilner, D. J., & Hayashi, M. 1999, ApJ, 518, L41

Ohishi, M., Irvine, W. M., & Kaifu, N. 1992, in Astrochemistry of Cosmic Phenomena, ed. P. D. Singh (Dordrecht: Kluwer), 171

Pavlyuchenkov, Y., Henning, T., & Wiebe, D. 2007, ApJ, 669, L101

Pavlyuchenkov, Y. N., & Shustov, B. M. 2004, Astronomy Reports, 48, 315

Pavlyuchenkov, Y. N., Shustov, B. M., Shematovich, V. I., Wiebe, D. S., & Li, Z.-Y. 2003, Astronomy Reports, 47, 176

Pavlyuchenkov, Y., Wiebe, D., Launhardt, R., & Henning, T. 2006, ApJ, 645, 1212

Peraiah, A. 2001, An Introduction to Radiative Transfer (Cambridge: Cambridge Univ. Press)

Rawlings, J. M. C., Hartquist, T. W., Menten, K. M., & Williams, D. A. 1992, MNRAS, 255, 471

Rawlings, J. M. C., & Yates, J. A. 2001, MNRAS, 326, 1423

Redman, M. P., Rawlings, J. M. C., Yates, J. A., & Williams D. A. 2004, MNRAS, 352, 243

Rohlfs, K., & Wilson, T. L. 2000, Tools of radio astronomy / New York : Springer, 2000

Schöier, F. L., van der Tak, F. F. S., van Dishoeck, E. F., & Black, J. H. 2005, A&A, 432, 369

Semenov, D., Wiebe, D., Henning, Th. 2004, A&A, 417, 93

Sohn, J., Won Lee, C., Park, Y.-S., Lee H. M., Myers, Ph. C., & Lee, Y. 2007, ApJ, 664, 928

Stenholm, L. G. 1980, A&AS, 42, 23

Tafalla, M., Myers, P. C., Caselli, P., Walmsley, C. M., & Comito, C. 2002, ApJ, 569, 815

Tafalla, M., Myers, P. C., Caselli, P., & Walmsley, C. M. 2004, Ap&SS, 292, 347

Tafalla, M., Santiago-García, J., Myers, P. C., Caselli, P., Walmsley, C. M., & Crapsi, A. 2006, A&A, 455, 577

Tsamis, Y. G., Rawlings, J. M. C., Yates, J. A., & Viti, S. 2008, ApJ, submitted.

van der Tak, F. F. S., Black, J. H., Schöier, F. L., Jansen, D. J., & van Dishoeck, E. F. 2007, A&A, 468, 627

Vasyunin, A. I., Sobolev, A. M., Wiebe, D. S., & Semenov, D. A. 2004, Astronomy Letters, 30, 566

van Zadelhoff, G.-J., et al. 2002, A&A, 395, 373

Young, K. E., Lee, J.-E., Evans, N. J., II, Goldsmith, P. F., & Doty, S. D. 2004, ApJ, 614, 252

Ward-Thompson, D., & Buckley, H. D. 2001, MNRAS, 327, 955

Wakelam, V., Herbst, E., & Selsis, F. 2006, A&A, 451, 551

Walker, Ch. K., Lada, Ch. J., Young, E. T., Maloney, Ph. R., Wilking, B. A. 1986, ApJ, 309, L47

Walker, C. K., Narayanan, G., & Boss, A. P. 1994, ApJ, 431, 767

Williams, J. P., Lee, C. W., & Myers, P. C. 2006, ApJ, 636, 952

Zhou, S. 1992, ApJ, 394, 204

Zhou, S., Evans, N. J., II, Koempe, C., Walmsley, C. M. 1993, ApJ, 404, 232

Zucconi, A., Walmsley, C. M., & Galli, D. 2001, A&A, 376, 650